CONF-9703144--

SANDIA REPORT

SAND97–8688
Unlimited Release
Printed September 1997

Influence of Pressure-Driven Gas Permeation on the Quasi-Steady Burning of Porous Energetic Materials

(Presented at the Seventh International Conference on Numerical Combustion/SIAM, York, UK, March 30–April 1, 1997)

Stephen B. Margolis

Prepared by
Sandia National Laboratories
Albuquerque, New Mexico 87185 and Livermore, California 94550

Sandia is a multiprogram laboratory operated by Sandia Corporation, a Lockheed Martin Company, for the United States Department of Energy under Contract DE-AC04-94AL85000.

Sandia National Laboratories

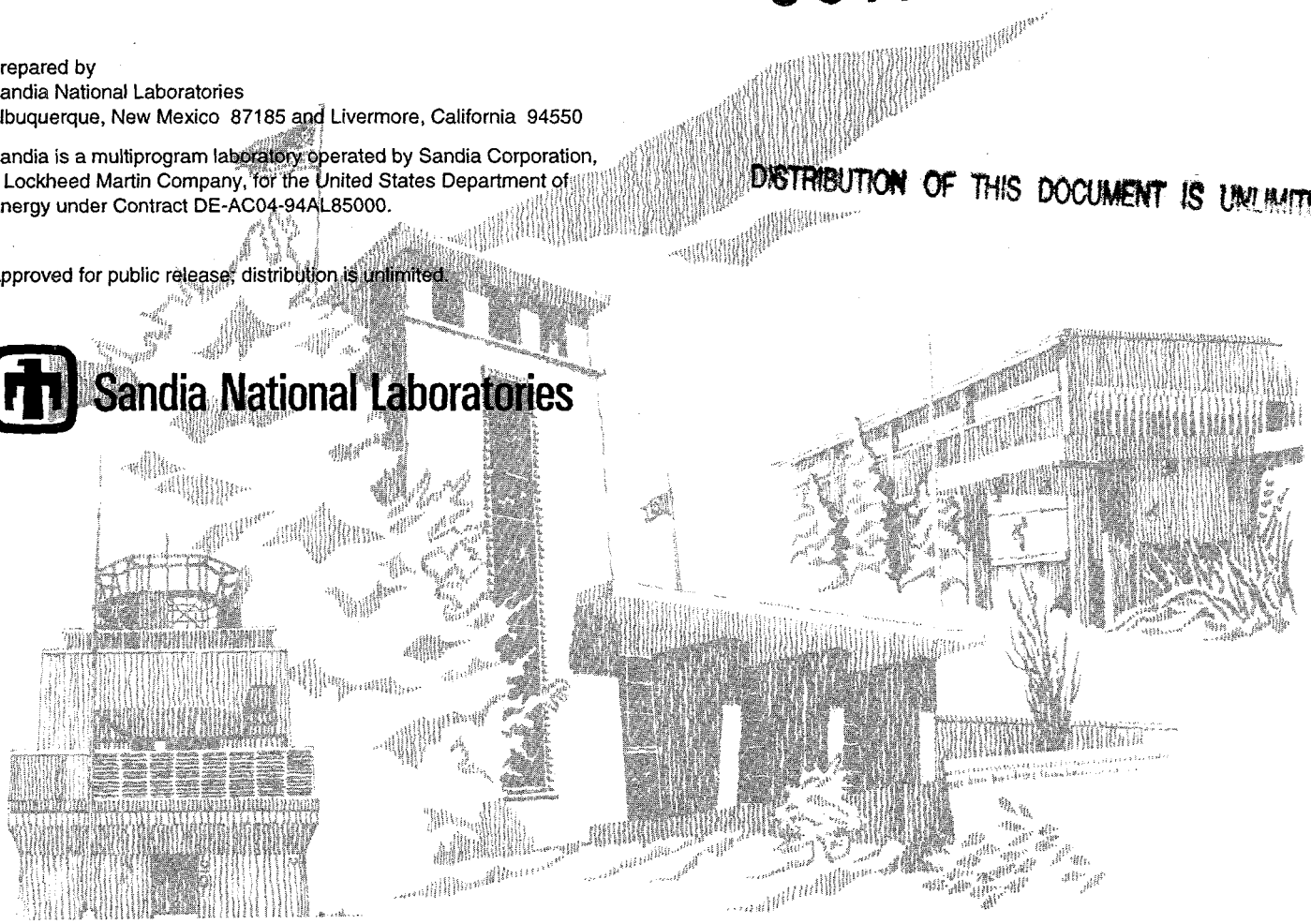

Issued by Sandia National Laboratories, operated for the United States Department of Energy by Sandia Corporation.

SAND97-8688 • UC-1409
Unlimited Release
Printed September 1997

INFLUENCE OF PRESSURE-DRIVEN GAS PERMEATION ON THE QUASI-STEADY BURNING OF POROUS ENERGETIC MATERIALS

STEPHEN B. MARGOLIS
Combustion Research Facility
Sandia National Laboratories
Livermore, California 94551-0969 USA

Abstract

A theoretical two-phase-flow analysis is developed to describe the quasi-steady propagation, across a pressure jump, of a multi-phase deflagration in confined porous energetic materials. The difference, or overpressure, between the upstream (unburned) and downstream (burned) gas pressure leads to a more complex structure than that which is obtained for an unconfined deflagration in which the pressure across the multi-phase flame region is approximately constant. In particular, the structure of such a wave is shown by asymptotic methods to consist of a thin boundary layer characterized by gas permeation into the unburned solid, followed by a liquid/gas flame region, common to both types of problems, in which the melted material is preheated further and ultimately converted to gaseous products. The effect of gas flow relative to the condensed material is shown to be significant, both in the porous unburned solid as well as in the exothermic liquid/gas melt layer, and is, in turn, strongly affected by the overpressure. Indeed, all quantities of interest, including the burned temperature, gas velocity and the propagation speed, depend on this pressure difference, leading to a significant enhancement of the burning rate with increasing overpressure. In the limit that the overpressure becomes small, the pressure gradient is insufficient to drive gas produced in the reaction zone in the upstream direction, and all gas flow relative to the condensed material is directed in the downstream direction, as in the case of an unconfined deflagration. The present analysis is particularly applicable to those types of porous energetic solids, such as degraded nitramine propellants, that can experience significant gas flow in the solid preheat region and which are characterized by the presence of exothermic reactions in a bubbling melt layer at their surfaces.

INFLUENCE OF PRESSURE-DRIVEN GAS PERMEATION ON THE QUASI-STEADY BURNING OF POROUS ENERGETIC MATERIALS

1. Introduction

The combustion behavior of porous energetic materials is of increasing interest due to the realization that even supposedly nonporous materials may develop significant porosities over time due either to aging or to other types of degradation that may arise from exposure to abnormal environments. In such materials, two-phase-flow effects are especially significant due to the presence of gas flow relative to the condensed material both within the unburned porous solid as well as in the exothermic liquid/gas layers that typically form on the surfaces of many types propellants (e.g., nitramines). In the presence of confinement, the significance of the convective transport effects due to two-phase flow are enhanced, leading, through gas permeation into the unburned solid, to a preheating of the solid and, consequently, to a strong enhancement of the burning rate relative to the unconfined case. Indeed, this type of preheating associated with gas permeation into the unburned solid is generally associated with the onset of specially identified modes of combustion, such as convective burning (cf. [1] and the references therein).

In the present work, we analyze, by means of asymptotic methods, certain effects of confinement on the deflagration structure and burning rate. In particular, we identify a quasi-steady propagation regime that is characterized by a leading boundary layer in the solid/gas region in which there is a rapid rise in pressure, followed by a liquid/gas region in which additional preheating and chemical reaction occur (Fig. 1). The pressure gradient in the boundary layer, in turn, drives gas produced in the reaction zone in the direction of the unburned solid, and thus one fundamental difference between the confined and unconfined cases is the direction of the gas flow in the solid/gas portion of the multi-phase flame structure. For this reason, this type of propagation mode that we seek to describe has been described in other types of flame-sheet analyses as a "gas-permeation boundary-layer" regime [2] by virtue of the fact that in sufficiently confined geometries, burning is enhanced by burned-gas permeation ahead of the reaction zone into the solid/gas preheat region.

The model used to investigate the wave structure described above is a modification of that derived previously [3], which, in turn, is essentially a simplified version of more general models of two-phase reacting flow (cf. [4]). In particular, the continuity and energy equations for each coexisting phase remain the same as in our previous study [3], as is the expression used for the liquid-phase velocity that, in turn, was motivated by liquid-phase momentum considerations [5]. However, the approximation of constant gas pressure, although appropriate under certain conditions for unconfined deflagrations, is clearly inadequate for the confined problem, which is characterized by a gas-phase pressure gradient in the solid/gas portion the multi-phase flame, and

a subsequent drag on the gas-phase velocity in the gas-permeation boundary layer. Accordingly, we phenomenologically relate the gas velocity to the pressure gradient in this layer by adopting Darcy's law for flow in a porous medium. As an additional simplification, however, we shall assume good thermal contact between coexisting phases and adopt the single-temperature approximation that the temperature at a given spatial location is the same for each phase. In keeping with our goal of focusing on two-phase-flow effects, we shall also deliberately simplify the chemistry by postulating the overall process $R(s) \longrightarrow R(l) \longrightarrow P(g)$, where the first step denotes the melting (assumed to be slightly endothermic) of the solid material, and the second represents a one-step exothermic process in which liquid-phase reactants are directly converted to burned gaseous products. For the present, we confine our attention to the case of a one-dimensional quasi-steady deflagration, leaving consideration of instability and other nonsteady and/or multidimensional effects for future work.

2. Formulation

A sketch of the physical problem is shown in Fig. 1. The unburned porous solid lies generally to the left, and the burned gas products lie to the right. The two are separated by a deflagration wave that moves from right to left, converting the former into the latter. These regions (unburned and burned) in turn are bounded on the left and right, respectively, but these boundaries are assumed to be sufficiently far away (relative to the width of the flame region) that the primary effect of confinement on the combustion wave itself is on the difference that develops between the upstream and downstream values of the pressure. In particular, the pressure becomes greater in the burned region (due to the production of gas via chemical reaction) than in the unburned solid, where, unlike the liquid/gas region, the drag on the gas flow associated with Darcy's law implies that the pressure sufficiently far upstream approaches its ambient value. The structure of the combustion wave thus consists of a solid/gas preheat region that contains a gas-permeation boundary layer in which the pressure rises from its ambient value to its larger (possibly much larger) value in the liquid/gas region, the melting surface that marks the left boundary of a liquid/gas preheat region (and the right boundary of the gas-permeation layer), the liquid/gas preheat zone, a relatively thin exothermic reaction layer in which chemical reaction occurs, and the burned region that extends to the right boundary. In the present work, we shall restrict attention to one spatial dimension ($\tilde{x}$), and use the subscripts s, l and g to denote solid, liquid and gas-phase quantities, respectively. Upstream conditions in the unburned porous solid are denoted by the subscript u, while downstream conditions in the product gases are identified by the subscript b. The appearance of a tilde over a symbol (e.g., $\tilde{x}$) denotes a dimensional quantity.

The governing system of equations are as follows. Denoting the melting surface that separates

the solid/gas and liquid/gas regions by $\tilde{x} = \tilde{x}_m$, and the gas-phase volume fraction by α, continuity in the region $\tilde{x} > \tilde{x}_m$ is expressed separately for the liquid and gas phases, where the latter may be replaced by an overall continuity equation for the two-phase medium. Consequently, we have

$$\frac{\partial}{\partial \tilde{t}}\left[(1-\alpha)\tilde{\rho}_l\right] + \frac{\partial}{\partial \tilde{x}}\left[(1-\alpha)\tilde{\rho}_l\tilde{u}_l\right] = -\tilde{A}\tilde{\rho}_l(1-\alpha)\exp\left(-\tilde{E}_l/\tilde{R}^\circ\tilde{T}\right), \quad \tilde{x} > \tilde{x}_m, \tag{1}$$

$$\frac{\partial}{\partial \tilde{t}}\left[(1-\alpha)\tilde{\rho}_l + \alpha\tilde{\rho}_g\right] + \frac{\partial}{\partial \tilde{x}}\left[(1-\alpha)\tilde{\rho}_l\tilde{u}_l + \alpha\tilde{\rho}_g\tilde{u}_g\right] = 0, \quad \tilde{x} > \tilde{x}_m. \tag{2}$$

where $\tilde{\rho}$, $\tilde{u}$, $\tilde{T}$ and $\tilde{t}$ denote density, velocity, the single temperature and time, respectively. For simplicity, we will assume a constant value for $\tilde{\rho}_l$, but not for $\tilde{\rho}_g$. In the reaction rate expression, $\tilde{E}_l$ is the overall activation energy, $\tilde{R}^\circ$ is the universal gas constant, and $\tilde{A}$ is the exponential reciprocal-time prefactor which, for simplicity, will be assumed constant. For this type of global kinetic modeling, however, it may be reasonable to assign a pressure, as well as a temperature, dependency to $\tilde{A}$. In the solid/gas region $\tilde{x} < \tilde{x}_m$, we assume for the solid phase a constant density $\tilde{\rho}_s$ and zero velocity ($\tilde{u}_s = 0$), with $\alpha \equiv \alpha_s$ also constant in this region. Gas-phase continuity for $\tilde{x} < \tilde{x}_m$ is thus independent of the solid phase and is given by

$$\frac{\partial \tilde{\rho}_g}{\partial \tilde{t}} + \frac{\partial}{\partial \tilde{x}}\left(\tilde{\rho}_g\tilde{u}_g\right) = 0, \quad \tilde{x} < \tilde{x}_m. \tag{3}$$

Conservation of energy for each phase in the liquid/gas and solid /gas regions is similarly given by separate equations for each coexisting phase, which, as before, may be summed to give an overall energy equation in each region. In the single-temperature limit, however, only the overall energy equations remain (cf. [3]) and these are given by

$$\begin{aligned}\frac{\partial}{\partial \tilde{t}}\left[\tilde{\rho}_l(1-\alpha)(\tilde{Q}+\tilde{c}_l\tilde{T}) + \tilde{\rho}_g\tilde{c}_g\alpha\tilde{T}\right] + \frac{\partial}{\partial \tilde{x}}\left[\tilde{\rho}_l\tilde{u}_l(1-\alpha)(\tilde{Q}+\tilde{c}_l\tilde{T}) + \tilde{\rho}_g\tilde{c}_g\tilde{u}_g\alpha\tilde{T}\right] \\ = \frac{\partial}{\partial \tilde{x}}\left[\tilde{\lambda}_l(1-\alpha)\frac{\partial \tilde{T}}{\partial \tilde{x}} + \tilde{\lambda}_g\alpha\frac{\partial \tilde{T}}{\partial \tilde{x}}\right] + \alpha\frac{\partial \tilde{p}_g}{\partial \tilde{t}}, \quad \tilde{x} > \tilde{x}_m,\end{aligned} \tag{4}$$

$$\begin{aligned}\frac{\partial}{\partial \tilde{t}}\left[\tilde{\rho}_s\tilde{c}_s(1-\alpha_s)\tilde{T} + \tilde{\rho}_g\tilde{c}_g\alpha_s\tilde{T}\right] + \frac{\partial}{\partial \tilde{x}}\left(\tilde{\rho}_g\tilde{c}_g\tilde{u}_g\alpha_s\tilde{T}\right) \\ = \frac{\partial}{\partial \tilde{x}}\left[\tilde{\lambda}_s(1-\alpha_s)\frac{\partial \tilde{T}}{\partial \tilde{x}} + \tilde{\lambda}_g\alpha_s\frac{\partial \tilde{T}}{\partial \tilde{x}}\right] + \alpha_s\frac{\partial \tilde{p}_g}{\partial \tilde{t}}, \quad \tilde{x} < \tilde{x}_m,\end{aligned} \tag{5}$$

where Eq. (1) has been used to eliminate the reaction-rate term in Eq. (4). Here, $\tilde{c}$, $\tilde{\lambda}$ and $\tilde{p}$ denote heat capacity (at constant volume for the liquid, and at constant pressure for the gas, both assumed constant), thermal conductivity and pressure, respectively, and $\tilde{Q}$ is the heat release for the global reaction at temperature $\tilde{T}$. We remark that because of the small Mach number and the small ratio of gas-to-condensed phase densities in the problems to be considered, no terms involving the pressures in the condensed phases appear in these equations, where the terms involving $\tilde{p}_g$ arises

from the contribution to the rate of change of the internal energy of the gas from the sum of the rate of surface work $-\partial(\alpha\tilde{u}_g\tilde{p}_g)/\partial\tilde{x}$ and the rate of volume work $-\tilde{p}_g\partial\alpha/\partial\tilde{t}$ performed by the gas.

Although analogous equations may be written for momentum conservation, we avoid introducing them explicitly by adopting certain simplifying approximations which are often used in these types of problems. In particular, in place of gas-phase momentum, we adopt Darcy's law in the solid/gas region, and assume, based on the small Mach number assumption, that the gas pressure is homogeneous in the liquid/gas region. If it is further assumed that the gas pressure in the burned region varies on a longer time scale than that associated with the flame structure itself (i.e., provided the confining boundary is sufficiently remote with respect to the flame), then the upstream and downstream pressures may be regarded as constant in the quasi-static sense. This argument is supported by the numerical calculations in [2], which led the authors of that study, which was based on a flame-sheet assumption, to delineate this quasi-steady regime as the "gas-permeation boundary-layer solution," so named because of the gas permeation in the solid/gas region, described later in the paper, that arises from the difference, or overpressure, between the upstream and downstream values of the gas pressure. Thus, in place of gas-phase momentum, we adopt the conditions

$$\tilde{u}_g = -\frac{\tilde{\kappa}(\alpha_s)}{\alpha_s\tilde{\mu}_g}\frac{\partial\tilde{p}_g}{\partial\tilde{x}}\,, \quad \tilde{x} < \tilde{x}_m\,; \qquad \tilde{p}_g = \tilde{p}_g^b\,, \quad \tilde{x} > \tilde{x}_m\,, \tag{6}$$

where $\tilde{\kappa}$ is the permeability of the solid/gas region and $\tilde{\mu}_g$ is the gas-phase viscosity. The gas itself is assumed to be ideal, and thus $\tilde{p}_g$ is coupled to the other field variables through the gas-phase equation of state,

$$\tilde{p}_g = \tilde{\rho}_g\tilde{R}^\circ\tilde{T}/\tilde{W}_g\,, \tag{7}$$

where $\tilde{W}_g$ is the molecular weight of the product gas. Consideration of condensed-phase momentum, on the other hand, leads in principle to an equation for the liquid-phase velocity $\tilde{u}_l$. Based on the analysis in [5], a reasonable first approximation is to set the condensed velocity equal the condensed mass burning rate divided by the condensed-phase density. In the present context, this implies that, since $\tilde{u}_s = 0$,

$$\tilde{u}_l = -\frac{d\tilde{x}_m}{d\tilde{t}}\left(\frac{\tilde{\rho}_s}{\tilde{\rho}_l} - 1\right)\,, \quad \tilde{x} > \tilde{x}_m\,, \tag{8}$$

where $d\tilde{x}_m/d\tilde{t} < 0$ is the (unknown) propagation velocity of the melting surface. A modification to this expression that introduces a linear dependence of $\tilde{u}_l$ on the gas-phase volume fraction α that qualitatively takes into account viscous and surface-tension-gradient (Marangoni) effects in the liquid/gas region was also proposed [5], but in the present work we shall adopt the simpler result given by Eq. (8).

The above equations now constitute a closed set for the variables α, $\tilde{u}_g$, $\tilde{T}$, $\tilde{\rho}_g$ and $\tilde{p}_g$. The problem is thus completely determined once initial and boundary conditions (including interface

relations at $\tilde{x} = \tilde{x}_m$) are specified. As in our previous study of the constant-pressure (unconfined) problem [3], we will not be concerned with the initial-value problem, but only the long-time solution corresponding to a (quasi-) steadily propagating deflagration. Thus, the required boundary conditions are given by

$$\alpha = \alpha_s \text{ for } \tilde{x} < \tilde{x}_m\,; \quad \tilde{u}_g \to 0\,, \quad \tilde{T} \to \tilde{T}_u\,, \quad \tilde{p}_g \to \tilde{p}_g^u \text{ as } \tilde{x} \to -\infty\,, \tag{9}$$

$$\tilde{p}_g = \tilde{p}_g^b \text{ for } \tilde{x} > \tilde{x}_m\,; \quad \alpha \to 1\,, \quad \tilde{u}_g \to \tilde{u}_g^b\,, \quad \tilde{T} \to \tilde{T}_b \text{ as } \tilde{x} \to +\infty\,, \tag{10}$$

where the burned temperature $\tilde{T}_b$ and burned gas velocity $\tilde{u}_g^b$ are to be determined, and the unburned and burned values $\tilde{\rho}_g^u$ and $\tilde{\rho}_g^b$ of the gas density follow from the equation of state. We remark that the upstream boundary condition on the gas velocity is in fact merely a consistency condition in the present formulation, since it is implied by the corresponding upstream condition on pressure and the first of Eqs. (6). Finally, denoting by $\pm$ superscripts quantities evaluated at $\tilde{x} = \tilde{x}_m^{\pm}$, the continuity and jump conditions across the melting surface are

$$\alpha^+ = \alpha^- = \alpha_s\,, \quad \tilde{u}_g^+ = \tilde{u}_g^- = -\frac{\tilde{\kappa}(\alpha_s)}{\alpha_s \tilde{\mu}_g} \frac{\partial \tilde{p}_g}{\partial \tilde{x}}\bigg|_{\tilde{x}=\tilde{x}_m^-}\,, \quad \tilde{p}_g^- = \tilde{p}_g^+ = \tilde{p}_g^b\,, \quad \tilde{T}^+ = \tilde{T}^- = \tilde{T}_m\,, \tag{11}$$

and, from conservation of enthalpy flux across $\tilde{x} = \tilde{x}_m$,

$$\begin{aligned} \left[(1-\alpha_s)\tilde{\lambda}_l + \alpha_s \tilde{\lambda}_g\right] \frac{d\tilde{T}}{d\tilde{x}}\bigg|_{\tilde{x}=\tilde{x}_m^+} - \left[\left[(1-\alpha_s)\tilde{\lambda}_s + \alpha_s \tilde{\lambda}_g\right] \frac{d\tilde{T}_s}{d\tilde{x}}\bigg|_{\tilde{x}=\tilde{x}_m^-}\right. \\ \left. = (1-\alpha_s)\tilde{\rho}_s \frac{d\tilde{x}_m}{d\tilde{t}} \left[\tilde{\gamma}_s + (\tilde{c}_s - \tilde{c}_l)\tilde{T}_m\right]\right., \end{aligned} \tag{12}$$

where $\tilde{\gamma}_s$ is the heat of melting of the solid at temperature $\tilde{T} = 0$ ($\tilde{\gamma}_s$ being negative when melting is endothermic).

3. Nondimensionalizations and the Quasi-Steady Problem

In the present work, we confine our attention to the case of a quasi-steady deflagration that propagates with the (unknown) speed $\tilde{U} = -d\tilde{x}_m/d\tilde{t}$, which is a convenient characteristic velocity for the problem. Assuming constant values for heat capacities and thermal conductivities, we then introduce the nondimensional variables

$$x = \frac{\tilde{\rho}_s \tilde{c}_s \tilde{U}}{\tilde{\lambda}_s} \tilde{x}\,, \quad t = \frac{\tilde{\rho}_s \tilde{c}_s \tilde{U}^2}{\tilde{\lambda}_s} \tilde{t}\,, \quad T_{s,l,g} = \frac{\tilde{T}_{s,l,g}}{\tilde{T}_u}\,, \quad u_{l,g} = \frac{\tilde{u}_{l,g}}{\tilde{U}}\,, \quad \rho_g = \frac{\tilde{\rho}_g}{\tilde{\rho}_g^u}\,, \quad p_g = \frac{\tilde{p}_g}{\tilde{p}_g^u} \tag{13}$$

where $\tilde{\rho}_g^u = \tilde{p}_g^u \tilde{W}_g / \tilde{R}^\circ \tilde{T}_u$ denotes the gas density at the unburned temperature $\tilde{T}_u$. In addition, the nondimensional parameters

$$\begin{aligned} &r = \frac{\tilde{\rho}_l}{\tilde{\rho}_s}\,, \quad \hat{r} = \frac{\tilde{\rho}_g^u}{\tilde{\rho}_s}\,, \quad l = \frac{\tilde{\lambda}_l}{\tilde{\lambda}_s}\,, \quad \hat{l} = \frac{\tilde{\lambda}_g}{\tilde{\lambda}_s}\,, \quad b = \frac{\tilde{c}_l}{\tilde{c}_s}\,, \quad \hat{b} = \frac{\tilde{c}_g}{\tilde{c}_s}\,, \quad \gamma_s = \frac{\tilde{\gamma}_s}{\tilde{c}_s \tilde{T}_u}\,, \quad Q = \frac{\tilde{Q}}{\tilde{c}_s \tilde{T}_u}\,, \\ &\kappa = \frac{\tilde{\rho}_s \tilde{c}_s \tilde{p}_g^u \tilde{\kappa}}{\tilde{\lambda}_s \tilde{\mu}_g}\,, \quad \hat{\pi} = \frac{\tilde{p}_g^u}{\tilde{\rho}_s \tilde{c}_s \tilde{T}_u} = \hat{r}\hat{b}\chi\,, \quad \chi = \frac{\gamma - 1}{\gamma}\,, \quad N = \frac{\tilde{E}_l}{\tilde{R}^\circ \tilde{T}_b}\,, \quad \Lambda = \frac{\tilde{\lambda}_s \tilde{A}}{\tilde{\rho}_s \tilde{c}_s \tilde{U}^2} e^{-N} \end{aligned} \tag{14}$$

are defined, where γ is the ratio of specific heats for the gas. It may be remarked that Λ is the appropriate burning-rate eigenvalue, the determination of which will provide the propagation speed $\tilde{U}$.

In nondimensional units, the propagation speed is minus unity. Hence, transforming to the moving coordinate $\xi = x + t$ whose origin is defined to be x_m, and introducing the above nondimensionalizations, steadily propagating deflagrations for the problem formulated in the previous section will be determined as solutions of the steady eigenvalue problem

$$\frac{d}{d\xi}\left[\rho_g(u_g+1)\right] = 0\,, \quad \xi < 0\,, \tag{15}$$

$$\frac{d}{d\xi}\left[r(1-\alpha)(u_l+1) + \hat{r}\alpha\rho_g(u_g+1)\right] = 0\,, \quad \xi > 0\,, \tag{16}$$

$$\frac{d}{d\xi}\left[(1-\alpha)(u_l+1)\right] = -\Lambda(1-\alpha)\exp\left[N\left(1-\frac{T_b}{T}\right)\right]\,, \quad \xi > 0\,, \tag{17}$$

$$(1-\alpha_s)\frac{dT}{d\xi} + \hat{r}\hat{b}\alpha_s\frac{d}{d\xi}\left[(u_g+1)\rho_g T\right] = \frac{d}{d\xi}\left[(1-\alpha_s+\hat{l}\alpha_s)\frac{dT}{d\xi}\right] + \hat{\pi}\alpha_s\frac{dp_g}{d\xi}\,, \quad \xi < 0\,, \tag{18}$$

$$\frac{d}{d\xi}\left[r(1-\alpha)(u_l+1)(Q+bT_l) + \hat{r}\hat{b}\alpha(u_g+1)\rho_g T\right] = \frac{d}{d\xi}\left\{\left[l(1-\alpha)+\hat{l}\alpha\right]\frac{dT}{d\xi}\right\}\,, \quad \xi > 0\,, \tag{19}$$

$$\rho_g T_g = p_g\,, \tag{20}$$

$$u_l = \frac{1}{r}(1-r)\,, \tag{21}$$

subject to the boundary and melting-surface conditions

$$\alpha = \alpha_s\,, \quad u_g = -\frac{\kappa(\alpha_s)}{\alpha_s}\frac{dp_g}{d\xi}\,, \text{ for } \xi < 0\,; \quad T \to 1\,, \quad p_g \to 1 \text{ as } \xi \to -\infty\,, \tag{22}$$

$$p_g = p_g^b \text{ for } \xi > 0\,; \quad \alpha \to 1\,, \quad u_g \to u_g^b\,, \quad T \to T_b \text{ as } \xi \to +\infty\,, \tag{23}$$

$$\alpha^+ = \alpha^- = \alpha_s\,, \quad u_g^+ = u_g^- = -\frac{\kappa(\alpha_s)}{\alpha_s\mu_g}\frac{dp_g}{d\xi}\bigg|_{\xi=0^-}\,, \quad p_g^- = p_g^+ = p_g^b\,, \quad T^+ = T^- = T_m\,, \tag{24}$$

$$\left[l(1-\alpha_s)+\hat{l}\alpha_s\right]\frac{dT}{d\xi}\bigg|_{\xi=0^+} - \left[1-\alpha_s+\hat{l}\alpha_s\right]\frac{dT}{d\xi}\bigg|_{\xi=0^-} = (1-\alpha_s)\left[-\gamma_s + (b-1)T_m\right]\,. \tag{25}$$

Thus, the final model for quasi-steady, planar deflagration that has been derived is given by Eqs. (15) – (25). We observe that ρ_g and u_l are readily eliminated from the problem by substituting Eqs. (20) and (21) into Eqs. (15) – (19), giving a simplified equation set for α, p_g, u_g and T as

$$\frac{d}{d\xi}\left[\frac{p_g}{T}(u_g+1)\right] = 0\,, \quad \xi < 0\,, \tag{26}$$

$$\frac{d}{d\xi}\left[(1-\alpha) + \hat{r}\alpha\frac{p_g}{T}(u_g+1)\right] = 0\,, \quad \xi > 0\,, \tag{27}$$

$$\frac{d}{d\xi}(1-\alpha) = -r\Lambda(1-\alpha)\exp\left[N\left(1-\frac{T_b}{T}\right)\right], \quad \xi > 0, \tag{28}$$

$$(1-\alpha_s)\frac{dT}{d\xi} + \hat{r}\hat{b}\alpha_s\frac{d}{d\xi}\left[p_g(u_g+1)\right] = \frac{d}{d\xi}\left[(1-\alpha_s+\hat{l}\alpha_s)\frac{dT}{d\xi}\right] + \hat{r}\hat{b}\chi\alpha_s\frac{dp_g}{d\xi}, \quad \xi < 0, \tag{29}$$

$$\frac{d}{d\xi}\left[(1-\alpha)(Q+bT) + \hat{r}\hat{b}\alpha p_g(u_g+1)\right] = \frac{d}{d\xi}\left\{\left[l(1-\alpha)+\hat{l}\alpha\right]\frac{dT}{d\xi}\right\}, \quad \xi > 0, \tag{30}$$

where the alternate expression for the coefficient $\hat{\pi}$ indicated in Eq. (14) has been used in the last term of Eq. (29).

4. Determination of T_b, u_g^b and $u_g(0)$

A partial solution in the region $\xi < 0$, where chemical activity is absent, as well as expressions for T_b, u_g^b and $u_g(0) = u_g|_{\xi=0}$, are obtained as follows. From Eqs. (26) and the boundary conditions (22), we have

$$p_g(u_g+1) = T, \quad \xi < 0, \tag{31}$$

and hence

$$u_g\big|_{\xi=0} = \frac{T_m}{p_g^b} - 1. \tag{32}$$

We observe from Eq. (31) that since $T \geq 1$, the gas velocity $u_g > -1$ in the gas/solid region $\xi < 0$. That is, consistent with a quasi-steady mode of burning, the speed of gas permeation into the solid must be less than the propagation speed of the deflagration. Equation (27) and the surface conditions (24) and (32) then imply

$$p_g^b(u_g+1) = \frac{\alpha + \alpha_s(\hat{r}-1)}{\hat{r}\alpha}T, \quad \xi > 0, \tag{33}$$

which, upon evaluation at $\xi = \infty$, determines u_g^b in terms of T_b as

$$u_g^b = \frac{1-\alpha_s+\hat{r}\alpha_s}{\hat{r}}\left(\frac{T_b}{p_g^b}\right) - 1. \tag{34}$$

Turning attention to the energy equations (29) and (30), we may readily perform a single integration and use the above relationships to obtain

$$(1-\alpha_s+\hat{r}\hat{b}\alpha_s)(T-1) = (1-\alpha_s+\hat{l}\alpha_s)\frac{dT}{d\xi} + \hat{r}\hat{b}\chi\alpha_s(p_g-1), \quad \xi < 0, \tag{35}$$

$$\left[b(1-\alpha)+\hat{b}(\alpha-\alpha_s+\hat{r}\alpha_s)\right]T = \left[l(1-\alpha)+\hat{l}\alpha\right]\frac{dT}{d\xi} - (1-\alpha)Q + \hat{b}(1-\alpha_s+\hat{r}\alpha_s)T_b, \quad \xi > 0. \tag{36}$$

Thus, subtracting Eq. (35) evaluated at $\xi = 0^-$ from Eq. (36) evaluated at $\xi = 0^+$ and using the jump condition (25), we obtain an expression for T_b given by

$$T_b = \frac{(1-\alpha_s)(Q+1+\gamma_s) + \hat{r}\hat{b}\alpha_s\left[1+\chi(p_g^b-1)\right]}{\hat{b}(1-\alpha_s+\hat{r}\alpha_s)}, \tag{37}$$

which, from Eq. (34), determines u_g^b as

$$u_g^b = \frac{1}{\hat{r}\hat{b}p_g^b}\left[(1-\alpha_s)(Q+1+\gamma_s-\hat{r}\hat{b}) - \hat{r}\hat{b}(p_g^b-1)(1-\alpha_s\chi)\right] . \tag{38}$$

We note that in the limit $p_g^b \to 1$, Eqs. (37) and (38) collapse to the previous results for unconfined burning, where in place of Darcy's law in the solid/gas region, the approximation $p_g = 1$ was used throughout. It is clear from these results that, since $0 < \chi = 1 - 1/\gamma < 1$, T_b increases linearly with the overpressure $p_g^b - 1$, as shown in Fig. 2. It is readily seen that for small overpressures T_b decreases with increasing values of the porosity α_s, whereas at higher overpressures, the opposite trend is observed. Indeed, denoting the burned temperature at zero porosity by $T_b^0 = (Q+1+\gamma_s)/\hat{b}$, which is independent of p_g^b, we obtain from Eq. (37) that for $\alpha_s > 0$, $T_b = T_b^0$ at the critical value of overpressure given by $p_g^b - 1 = (T_b^0 - 1)/\chi$. For overpressures greater than this critical value, the preheating effect due to gas permeation is sufficient to overcome that due to a decrease in the amount of solid material, resulting in an increase in burned temperature above T_b^0. It is clear from Fig. 2 that the magnitude of the difference $T_b - T_b^0$ at a given value of the overpressure is an increasing function of α_s. In connection with this result, we observe from Eq. (38) and Fig. 3 that the burned gas velocity u_g^b is a monotonically decreasing function of the overpressure. In fact, for sufficiently large overpressures that satisfy the condition

$$p_g^b - 1 > \frac{1-\alpha_s}{1-\alpha_s\chi}\left(\frac{Q+1+\gamma_s}{\hat{r}\hat{b}} - 1\right) = \frac{(1-\alpha_s)(T_b^0-\hat{r})}{\hat{r}(1-\alpha_s\chi)} , \tag{39}$$

which depends on α_s, we find that u_g^b is negative, implying a gas flow in the upstream direction throughout the multi-phase flame. This is clearly illustrated in Fig. 3, which shows the curves for u_g^b as a function of $p_g^b - 1$ crossing the horizontal axis at the above critical value of the overpressure. Also shown in Fig. 3 is the value of the gas velocity $u_g(\xi)$ at the solid/liquid interface $\xi = 0$, which is only positive for relatively small values of the overpressure. In particular, from Eq. (32), $u_g(0)$ crosses the horizontal axis at the critical value $p_g^b - 1 = T_m - 1$, beyond which gas flow is directed into the solid/gas region, resulting in the preheating effect due to gas permeation as described above. Further solution of the problem in the liquid/gas region, which is necessary for the determination of the burning-rate eigenvalue, is considered in the following section.

Before proceeding with an analysis of the liquid/gas reaction reaction region, we observe that the problem in the solid/gas region can be reduced to a scalar problem for the gas pressure p_g. In particular, from Eq. (31) and the Darcy formula for u_g in Eq. (22), T and thus u_g are given in terms of p_g by

$$T = p_g\left(1 - \frac{\kappa}{\alpha_s}\frac{dp_g}{d\xi}\right) , \quad u_g = \frac{T}{p_g} - 1 , \quad \xi < 0 . \tag{40}$$

Substituting these results into Eq. (35) thus yields a second-order equation for p_g in the region $\xi < 0$ given by

$$(1-\alpha_s+\hat{r}\hat{b}\alpha_s)\left[p_g\left(1-\frac{\kappa}{\alpha_s}\frac{dp_g}{d\xi}\right)-1\right]=(1-\alpha_s+\hat{l}\alpha_s)\frac{d}{d\xi}\left[p_g\left(1-\frac{\kappa}{\alpha_s}\frac{dp_g}{d\xi}\right)\right]+\hat{r}\hat{b}\chi\alpha_s(p_g-1)\,, \quad (41)$$

subject to the boundary conditions

$$p_g = p_g^b\,, \quad \frac{dp_g}{d\xi}=\frac{\alpha_s}{\kappa}\left(1-\frac{T_m}{p_g^b}\right) \text{ at } \xi=0\,; \quad p_g \to 1 \text{ as } \xi \to -\infty\,, \quad (42)$$

where the second condition follows from the Darcy formula and Eq. (32) for u_g evaluated at $\xi = 0$. We note that the last condition, aside from being consistent with the first of Eqs. (40), is already built into Eq. (41) by virtue of the fact that Eq. (41) is really a first integral of Eq. (29). Had the above expression for T been substituted directly into the latter, a third-order equation for p_g would have been obtained, permitting the specification of the three boundary conditions (42). The problem (41) – (42), the solution of which will determine T and u_g according to Eqs. (40), will be treated in the section following the determination of the burning-rate eigenvalue.

5. The Burning-Rate Eigenvalue

In order to determine the burning-rate eigenvalue, we must complete our analysis of the liquid/gas region $\xi > 0$. In this regard, Eqs. (28) and (36) constitute two equations for T and α in this region, with u_g then determined by Eq. (33) and the eigenvalue Λ determined by the boundary conditions. In order to handle the Arrhenius nonlinearity, we exploit the largeness of the nondimensional activation energy N and analyze the problem in the asymptotic limit $N \gg 1$. Since $p_g = p_g^b$ in the liquid/gas region, the analysis below follows closely that given in [3] for the unconfined problem.

In the limit $N \to \infty$, all chemical activity is concentrated in a very thin region where T is within $O(1/N)$ of T_b. Denoting the location of this thin zone by $\xi_r > 0$, we see that the semi-infinite liquid/gas region is comprised of a preheat zone ($0 < \xi < \xi_r$) where chemical activity is exponentially small, the thin reaction zone where the chemical reaction goes to completion, and a burned region $\xi > \xi_r$. Thus, we conclude from Eq. (28) that

$$\alpha = \begin{cases} \alpha_s, & \xi < \xi_r \\ 1, & \xi > \xi_r\,, \end{cases} \quad (43)$$

and from Eqs. (33) and (34),

$$u_g = \begin{cases} T/p_g^b - 1, & \xi < \xi_r \\ \hat{r}^{-1}(1-\alpha_s+\hat{r}\alpha_s)T_b/p_g^b - 1 = u_g^b, & \xi > \xi_r\,, \end{cases} \quad (44)$$

Since T is within $O(1/N)$ of T_b in the reaction zone, the analysis of this thin region requires the use of a stretched coordinate (see below). As a result, T is continuous with respect to the $O(1)$ outer variable ξ at $\xi = \xi_r$, and thus the gas velocity jumps across $\xi = \xi_r$ by the amount

$$u_g\big|_{\xi=\xi_r^+} - u_g\big|_{\xi=\xi_r^-} = \frac{1}{\hat{r}}(1-\hat{r})(1-\alpha_s)\frac{T_b}{p_g^b}\,, \tag{45}$$

which is positive assuming the unburned gas density is less than that of the solid (i.e., $\hat{r} < 1$). Finally, using Eq. (43), Eq. (36) may be integrated a second time to completely determine the outer temperature profile in the liquid/gas region as

$$T(\xi) = \begin{cases} B + (T_m - B)\exp\left[\dfrac{b(1-\alpha_s) + \hat{r}\hat{b}\alpha_s}{l(1-\alpha_s) + \hat{l}\alpha_s}\xi\right], & 0 < \xi < \xi_r \\ T_b\,, & \xi > \xi_r\,, \end{cases} \tag{46}$$

where

$$B \equiv \frac{(1-\alpha_s)(1+\gamma_s) + \hat{r}\hat{b}\alpha_s\left[1 + \chi(p_g^b - 1)\right]}{b(1-\alpha_s) + \hat{r}\hat{b}\alpha_s}\,. \tag{47}$$

We note that $T(\xi)$ for $\xi < 0$ is still to be determined from Eq. (40) and the solution of the pressure problem (41) – (42), as described in the next section; however, it is not required for the determination of the burning-rate eigenvalue Λ. The location ξ_r of the reaction zone, which appears as a sheet on the scale of the outer variable ξ, is thus determined by Eqs. (46) from continuity of T as

$$\xi_r = \frac{l(1-\alpha_s) + \hat{l}\alpha_s}{b(1-\alpha_s) + \hat{r}\hat{b}\alpha_s}\ln\left(\frac{T_b - B}{T_m - B}\right). \tag{48}$$

The determination of the burning-rate eigenvalue Λ, as well as the spatial evolution of the variables α and u_g (which are discontinuous on the scale of the outer variable ξ), requires an analysis of the thin reaction-zone region in the vicinity of ξ_r. We thus introduce a stretched inner variable η and a normalized temperature variable Θ defined by

$$\Theta = \frac{T-1}{T_b - 1}\,, \qquad \eta = \beta(\xi - \xi_r)\,, \quad \beta \equiv (1 - T_b^{-1})N \gg 1\,, \tag{49}$$

where β is the Zel'dovich number, and seek solutions in the form of the expansions

$$\begin{aligned} &\alpha \sim \alpha_0 + \beta^{-1}\alpha_1 + \beta^{-2}\alpha_2 + \cdots\,, \quad u_g \sim u_0 + \beta^{-1}u_1 + \beta^{-2}u_2 + \cdots\,, \\ &\Theta \sim 1 + \beta^{-1}\theta_1 + \beta^{-2}\theta_2 + \cdots\,, \qquad \Lambda \sim \beta(\Lambda_0 + \beta^{-1}\Lambda_1 + \beta^{-2}\Lambda_2 + \cdots)\,. \end{aligned} \tag{50}$$

The coefficients in the expansion of u_g are readily determined from Eq. (33) in terms of the α_i and θ_i, which themselves are obtained from solving the sequence of inner problems that arise from substituting the above expansions into Eqs. (28) and (36) and matching with the outer solutions for $\xi < \xi_r$ and $\xi > \xi_r$. In particular, at leading order the inner problem is given by

$$\frac{d\alpha_0}{d\eta} = r\Lambda_0(1-\alpha_0)\,e^{\theta_1}\,, \tag{51}$$

$$\left[l+(\hat{l}-l)\alpha_0\right]\frac{d\theta_1}{d\eta}=\frac{D}{T_b-1}(1-\alpha_0)\,, \tag{52}$$

subject to the matching conditions

$$\alpha_0\to\alpha_s\,,\quad \theta_1\sim E\eta \text{ as } \eta\to-\infty\,, \tag{53}$$

$$\alpha_0\to 1\,,\quad \theta_1\to 0 \text{ as } \eta\to+\infty\,. \tag{54}$$

Here, D and E are defined as

$$D\equiv(b-\hat{b})T_b+Q\,,\qquad E\equiv\frac{1}{T_b-1}\frac{dT}{d\xi}\bigg|_{\xi=\xi_r^-}\,, \tag{55}$$

where the latter is calculated from Eq. (46).

The problem (51) - (54) is identical in form to that obtained for the corresponding unconfined problem [3], and is readily solved by employing α_0 as the independent variable. Thus, using Eq. (51), Eq. (52) may be written as

$$r\Lambda_0\left[l+(\hat{l}-l)\alpha_0\right]e^{\theta_1}\frac{d\theta_1}{d\alpha_0}=\frac{D}{T_b-1}\,, \tag{56}$$

which is readily integrated from α_s (at $\eta=-\infty$) to any $\alpha_0\le 1$ to give

$$e^{\theta_1(\alpha_0)}=\frac{D}{(T_b-1)r\Lambda_0}\int_{\alpha_s}^{\alpha_0}\frac{d\alpha_0}{l+(\hat{l}-l)\alpha_0}\,. \tag{57}$$

Evaluating the latter at $\alpha_0=1$ (at which $\theta_1=0$) thus determines the leading-order coefficient Λ_0 in the expansion of the burning-rate eigenvalue as

$$\Lambda_0=\begin{cases}\dfrac{D}{(T_b-1)r(\hat{l}-l)}\ln\left[\dfrac{\hat{l}}{l+(\hat{l}-l)\alpha_s}\right], & l\neq\hat{l}\\[2ex] \dfrac{D}{(T_b-1)rl}(1-\alpha_s)\,, & l=\hat{l}\,,\end{cases} \tag{58}$$

and using this result in Eq. (57) for arbitrary α_0 then determines $\theta_1(\alpha_0)$ as

$$\theta_1(\alpha_0)=\begin{cases}\ln\left(\dfrac{\ln\left[l+(\hat{l}-l)\alpha_0\right]-\ln\left[l+(\hat{l}-l)\alpha_s\right]}{\ln\hat{l}-\ln\left[l+(\hat{l}-l)\alpha_s\right]}\right), & \hat{l}\neq l\\[2ex] \ln\left(\dfrac{\alpha_0-\alpha_s}{1-\alpha_s}\right), & \hat{l}=l\,.\end{cases} \tag{59}$$

The determination of $\alpha_0(\eta)$, and hence $\theta_1(\eta)$, then follows directly from Eq. (51).

From Eq. (58) and the definition of Λ [see the last of Eqs. (14) and (50)], the leading-order expression for the dimensional propagation speed $\tilde{U}$ is given by

$$\tilde{U}^2\sim\frac{r(T_b-1)\tilde{A}(p_g^b)}{\beta D\tilde{\rho}_s\tilde{c}_s}e^{-N}\cdot\tilde{f}(\tilde{\lambda}_g,\tilde{\lambda}_l)=\frac{rT_b^2}{(b-\hat{b})T_b+Q}\frac{\tilde{A}(p_g^b)}{\tilde{\rho}_s\tilde{c}_s}e^{-N_u/T_b}\cdot\tilde{f}(\tilde{\lambda}_g,\tilde{\lambda}_l)\,, \tag{60}$$

where $N_u = \tilde{E}_l/\tilde{R}^\circ\tilde{T}_u = NT_b$ is independent of T_b and the last factor, which contains the complete dependence of the burning rate on the thermal conductivities, is given by

$$\tilde{f}(\tilde{\lambda}_g, \tilde{\lambda}_l) = \begin{cases} \dfrac{\tilde{\lambda}_g - \tilde{\lambda}_l}{\ln\left(\tilde{\lambda}_g/[\tilde{\lambda}_l + (\tilde{\lambda}_g - \tilde{\lambda}_l)\alpha_s]\right)}, & \tilde{\lambda}_g \neq \tilde{\lambda}_l \\ \tilde{\lambda}_l/(1-\alpha_s), & \tilde{\lambda}_g = \tilde{\lambda}_l . \end{cases} \tag{61}$$

The expression (60) for the burning rate, though identical in form to that obtained for the case of constant pressure [3], nonetheless differs implicitly from that result through the linear dependence of T_b on the overpressure $p_g^b - 1$.

In order to analyze the dependence of the burning rate on the overpressure, it is convenient to define the normalized burning rate $U^* = \tilde{U}(p_g^b)/\tilde{U}(1)$, where the argument denotes the value of p_g^b. Consequently, from Eq. (60), we obtain $U^* = U_n[\tilde{A}(p_g^b)/\tilde{A}(1)]^{1/2}$, where the coefficient U_n is given by

$$U_n = \frac{T_b(p_g^b)}{T_b(1)}\left[\frac{(b-\hat{b})T_b(1)+Q}{(b-\hat{b})T_b(p_g^b)+Q}\right]^{1/2} \exp\left[\frac{N_u}{2}\left(\frac{1}{T_b(1)} - \frac{1}{T_b(p_g^b)}\right)\right], \tag{62}$$

and where T_b as a function of p_g^b is given by Eq.(37). In this form, it is readily seen, since T_b is a linearly increasing function of overpressure and the nondimensional activation-energy parameter N_u is typically very large (note the definition of N_u is in terms of the *unburned* temperature T_u), that U_n is exponentially sensitive to T_b and hence p_g^b as the overpressure $p_g^b - 1$ increases from zero. Thus, as the overpressure increases, the burning rate increases exponentially (Fig. 4), reflecting the sensitivity to the corresponding increase in the rate of gas permeation into the solid/gas region given by Eq. (32). We remark that this result cannot be predicted with the type of constant-pressure model appropriate for unconfined deflagrations [3], since in that case, the gas flow is always in the downstream direction (if one imposes the upstream boundary condition that u_g vanish) and an increase in pressure serves to decrease T_b due to the increase in the gas density ($\hat{r}$ increases) that absorbs more of the heat of reaction. In the present context, the upstream gas density $\hat{r}$ remains constant, and an increase in overpressure serves to preheat the unburned solid through enhanced permeation of the burned gas into the solid/gas region. In the limit of large overpressures, T_b^{-1} becomes small and the exponential factor in Eq. (62) approaches a constant value. Consequently, in the range of large overpressures, the dependence of U_n on p_g^b becomes algebraic. This is also illustrated in Fig. 4, in which case (since $b = \hat{b}$) the saturated dependence of U_n on p_g^b is linear. We note that this feature (exponential transition to an algebraic pressure-dependent burning rate) is qualitatively consistent with most experiments in Crawford-type (large volume) bombs that indicate a rapid increase in the burning rate frequently associated with the onset of convective burning (cf. [2],[6]), followed by a less dramatic pressure dependence that is typically represented in the form Ap^n.

6. Analysis of the Gas-Permeation Layer

Although the calculation of the burning-rate eigenvalue in the previous section did not require a detailed knowledge of the actual solution profiles in the solid/gas region [due to the fact that it was sufficient to determine the results (31) – (32) for u_g], it is nonetheless of interest to compute those solutions to better understand the effect of an overpressure on gas permeation into the unburned porous solid. It is thus convenient to define the overpressure $p = p_g - 1$, in terms of which the pressure problem (41) – (42) can be written as

$$(1-\alpha_s+\hat{r}\hat{b}\alpha_s)\left[p-\frac{\kappa}{\alpha_s}(p+1)\frac{dp}{d\xi}\right]=(1-\alpha_s+\hat{l}\alpha_s)\frac{d}{d\xi}\left[p-\frac{\kappa}{\alpha_s}(p+1)\frac{dp}{d\xi}\right]+\hat{r}\hat{b}\chi\alpha_s p\,, \tag{63}$$

subject to

$$p=p_b=p_g^b-1\,,\quad \frac{dp}{d\xi}=\frac{\alpha_s}{\kappa}\left(1-\frac{T_m}{p_b+1}\right)\ \text{ at }\ \xi=0\,;\quad p\to 0\ \text{ as }\ \xi\to-\infty\,. \tag{64}$$

Since our goal is a qualitative understanding of gas-permeation effects, it suffices to obtain approximate solutions using asymptotic methods. In particular, we introduce a bookkeeping parameter $\epsilon \ll 1$ and consider the realistic parameter regime in which $\hat{r}$, $\hat{l}$, α_s, and κ/α_s are all $O(\epsilon)$, where we note that the permeability κ is usually proportional to some power of α_s that is greater than unity (cf. [4,7]). That is, we scale these small quantities as

$$\alpha_s=\alpha_s^*\epsilon\,,\quad \kappa=\kappa^*\epsilon^2\,,\quad \hat{r}=\hat{r}^*\epsilon\,,\quad \hat{l}=\hat{l}^*\epsilon\,, \tag{65}$$

in terms of which Eqs. ((63) and (64) become

$$(1-\epsilon\alpha_s^*+\epsilon^2\hat{r}^*\hat{b}\alpha_s^*)\left[p-\epsilon\frac{\kappa^*}{\alpha_s^*}(p+1)\frac{dp}{d\xi}\right]=(1-\epsilon\alpha_s^*+\epsilon^2\hat{l}^*\alpha_s^*)\frac{d}{d\xi}\left[p-\epsilon\frac{\kappa^*}{\alpha_s^*}(p+1)\frac{dp}{d\xi}\right]+\epsilon^2\hat{r}^*\hat{b}\chi\alpha_s^* p\,, \tag{66}$$

$$p=p_b=p_g^b-1\,,\quad \frac{dp}{d\xi}=\epsilon^{-1}\frac{\alpha_s^*}{\kappa^*}\left(1-\frac{T_m}{p_b+1}\right)\ \text{ at }\ \xi=0\,;\quad p\to 0\ \text{ as }\ \xi\to-\infty\,. \tag{67}$$

We now proceed to obtain asymptotic solutions for two primary cases of interest.

(i) $p_b \sim O(1)$:

For $O(1)$ overpressures, the second condition in Eq. (67) suggests that there is an $O(\epsilon)$ boundary layer in the vicinity of $\xi = 0$. Accordingly, we introduce the stretched coordinate $\eta = \xi/\epsilon$ and seek the boundary-layer, or inner, solution in the form $p = p^i \sim p_0 + \cdots$. In terms of these variables, the leading-order version of Eqs. (66) and (67) in the boundary layer is thus given by

$$\frac{d}{d\eta}\left[p_0-\frac{\kappa^*}{\alpha_s^*}(p_0+1)\frac{dp_0}{d\eta}\right]=0\,, \tag{68}$$

$$p_0 = p_b\,, \quad \frac{dp_0}{d\eta} = \frac{\alpha_s^*}{\kappa^*}\left(1 - \frac{T_m}{p_b + 1}\right) \quad \text{at} \quad \eta = 0\,, \tag{69}$$

where only the first two conditions in Eq. (67) apply to the boundary-layer solution. Integrating Eq. (68) twice and applying the above conditions at $\eta = 0$, we obtain an implicit solution for p_0 as

$$\frac{\alpha_s^*}{\kappa^*}\eta = p_0 - p_b + T_m \ln\left(\frac{p_0 - T_m + 1}{p_b - T_m + 1}\right). \tag{70}$$

Denoting this solution by $p_0(\eta)$, we note that since $p_0 \to T_m - 1 > 0$ as $\eta \to -\infty$, the inner solution cannot satisfy the last boundary condition in Eq. (67). Thus it is necessary to construct an outer solution $p = p^o \sim q_0 + \cdots$ on the scale of the outer variable ξ. From Eq. (66), the equation for q_0 is given by

$$q_0 = \frac{dq_0}{d\xi}\,, \tag{71}$$

or $q_0 = c_1\, e^{\xi}$. This clearly satisfies the outer boundary condition at $\xi = -\infty$, whereas the requirement that it match with the inner solution (70) as $\xi \to 0$ determines that the integration constant $c_1 = \lim_{\eta \to -\infty} q_0(\eta) = T_m - 1$. Thus,

$$q_0 = (T_m - 1)e^{\xi}\,, \tag{72}$$

and a leading-order, uniformly-valid composite solution is given by

$$p = p^o + p^i - \lim_{\xi \to 0} p^0 \sim p_0(\xi/\epsilon) + (T_m - 1)(e^{\xi} - 1)\,, \tag{73}$$

where the leading-order inner solution p_0 has been functionally expressed in terms of the outer variable ξ. The above inner, outer and composite solutions are illustrated in Fig. 5. From Eq. (73) and the first integral of Eq. (68), the gas velocity in the solid/gas region is, in turn, given by

$$u_g = -\frac{\kappa}{\alpha_s}\frac{dp}{d\xi} \sim -1 + \frac{T_m}{p_0(\xi/\epsilon) + 1} - \epsilon\frac{\kappa^*}{\alpha^*}(T_m - 1)\, e^{\xi}\,, \tag{74}$$

which, being the derivative of a leading-order approximation, is correct to O(1), with an O(ϵ) error at $\xi = 0$ [see Eq. (32)]. We observe that $p_0(\xi/\epsilon) \to T_m - 1$ as ξ approaches O(1) negative values, and thus, as indicated in Fig. 5, it is clear that gas permeation for O(1) overpressures is only significant in the thin boundary layer adjacent to the solid/liquid interface, assuming $p_b > T_m - 1$. Although this last qualification is by far the typical case (since $T_m - 1 = \tilde{T}_m/\tilde{T}_u - 1$ is not likely to be larger than unity), it is nonetheless of interest to point out that the structure of the solution will change as p_b approaches the value $T_m - 1$ due to the fact that the gradient of pressure at $\xi = 0$, which has been scaled as O(ϵ^{-1}) in Eq. (67), will cease to be large in that limit. Indeed, for small overpressures ($0 < p_b < T_m - 1$), the pressure gradient becomes negative at $\xi = 0$, indicating,

according to Eqs. (22) and (32), a gas flow out of the solid in the downstream direction, as in the case of an unconfined deflagration analyzed previously under the constant-pressure approximation [3].

(ii) $p_b \sim \mathrm{O}(\epsilon^{-1}) \gg 1$:

The other primary case of interest in many applications is the limit in which the overpressure itself becomes large. In that case, it is useful to rescale p in Eqs. (66) and (67) by defining the scaled overpressure $P = \epsilon p$. In terms of P, Eqs. (66) and (67) become

$$(1-\epsilon\alpha_s^*+\epsilon^2\hat{r}^*\hat{b}\alpha_s^*)\left[P-\frac{\kappa^*}{\alpha_s^*}(P+\epsilon)\frac{dP}{d\xi}\right] = (1-\epsilon\alpha_s^*+\epsilon^2\hat{l}^*\alpha_s^*)\frac{d}{d\xi}\left[P-\frac{\kappa^*}{\alpha_s^*}(P+\epsilon)\frac{dP}{d\xi}\right]+\epsilon^2\hat{r}^*\hat{b}\chi\alpha_s^*P)\,, \tag{75}$$

$$P = P_b \equiv \frac{1}{\epsilon}(p_g^b - 1)\,, \quad \frac{dP}{d\xi} = \frac{\alpha_s^*}{\kappa^*}\left(1-\frac{\epsilon T_m}{P_b+\epsilon}\right) \text{ at } \xi = 0\,; \quad P \to 0 \text{ as } \xi \to -\infty\,. \tag{76}$$

Since there is now no reason to suspect a boundary layer near $\xi = 0$, we seek a straightforward perturbation solution on the ξ - scale as $P = P^o \sim P_0 + \cdots$. From Eq. (75), the leading-order problem for P_0 is thus given by

$$P_0 - \frac{\kappa^*}{\alpha_s^*}P_0\frac{dP_0}{d\xi} = \frac{d}{d\xi}\left(P_0 - \frac{\kappa^*}{\alpha_s^*}P_0\frac{dP_0}{d\xi}\right)\,, \tag{77}$$

$$P_0 = P_b\,, \quad \frac{dP_0}{d\xi} = \frac{\alpha_s^*}{\kappa^*} \text{ at } \xi = 0\,; \quad P_0 \to 0 \text{ as } \xi \to -\infty\,. \tag{78}$$

A single integration of Eq. (77) gives

$$P_0 - \frac{\kappa^*}{\alpha_s^*}P_0\frac{dP_0}{d\xi} = c_1 e^{\xi}\,, \tag{79}$$

where the boundary conditions (78) at $\xi = 0$ require that the integration constant $c_1 = 0$. In that case, Eq. (79) implies two possible solutions, namely

$$P_0 = 0 \quad \text{or} \quad P_0 = \frac{\alpha_s^*}{\kappa^*}\xi + c_2\,, \tag{80}$$

where the first solution satisfies the boundary condition at $\xi = -\infty$ and the second satisfies the conditions at $\xi = 0$ provided we choose $c_2 = P_b$. Since negative values of pressure are unphysical, a continuous solution is given by

$$P_0 = \begin{cases} (\alpha_s^*/\kappa^*)(\xi+\xi_0)\,, & -\xi_0 < \xi \le 0 \\ 0\,, & \xi < -\xi_0 \end{cases}\,, \quad \xi_0 = \frac{\kappa^*}{\alpha_s^*}P_b\,, \tag{81}$$

which is valid everywhere except at $\xi = -\xi_0$ where the derivative is discontinuous. This kink in the solution thus suggests the existence of a thin corner layer in that vicinity. Hence, we interpret Eq. (81) as the leading-order outer solution, and proceed to construct an inner solution in a thin region

centered about $\xi = -\xi_0$. In particular, we now define the inner variable $\eta = \epsilon^{-\delta}(\xi + \xi_0)$ and seek a solution of the form $P = P^i \sim \epsilon^\sigma(p_0 + \cdots)$, where the latter scaling reflects the expectation that P is small in the corner layer, with $\delta > 0$ and $\sigma > 0$ to be determined. Substituting these inner variables into Eq. (75), we determine that the ability to match the inner solution with the outer solution on either side of the corner layer requires that $\delta = \sigma = 1$. In that case, the leading-order equation for p_0 is given by

$$\frac{d}{d\eta}\left[p_0 - \frac{\kappa^*}{\alpha^*}(p_0 + 1)\frac{dp_0}{d\eta}\right] = 0\,, \tag{82}$$

the general solution of which is given by

$$\frac{\alpha_s^*}{\kappa^*}\eta + c_2 = p_0 + (c_1 + 1)\ln(p_0 - c_1)\,, \tag{83}$$

where c_1 and c_2 are constants of integration. It is clear that $p_0 \to c_1$ as $\eta = -\infty$, thereby requiring the choice $c_1 = 0$ in order that this solution match with the outer solution (81) for $\xi < -\xi_0$. On the other hand, the one-term outer expansion of the inner solution (83), written in terms of the outer variables, is given by $P = (\alpha_s^*/\kappa^*)(\xi + \hat{\xi}_0)$, which is identical to the outer solution (81) for $\xi > -\xi_0$. Thus, the leading-order composite solution is, in fact, the inner solution (83), which, when written in the outer variables, becomes

$$\frac{\alpha_s^*}{\kappa^*}(\xi + \xi_0) \sim P + \epsilon \ln\left(\frac{P}{\epsilon}\right) - \epsilon c_2\,, \tag{84}$$

where c_2 is still undetermined. Although Eq. (84) is a valid leading-order approximation, we observe that the error at $\xi = 0$ is $O(\epsilon \ln \epsilon)$, since the exact boundary condition is $P = P_b$ at $\xi = 0$. Consequently, it is clear that higher-order approximations would involve terms of this magnitude so as to satisfy this boundary condition. Examining Eq. (84), we may anticipate this development by setting $c_2 = \ln(P_b/\epsilon)$, giving rise an enhanced approximation of the form

$$\frac{\alpha_s^*}{\kappa^*}(\xi + \xi_0) \sim P + \epsilon \ln\left(\frac{P}{P_b}\right)\,. \tag{85}$$

The outer and composite solutions (81) and (85) for the scaled overpressure P are illustrated in Fig. 6. It is clear that in this case, gas permeation extends an O(1) distance into the gas/solid region, although, as in the previous case of O(1) overpressures, the extent of gas permeation remains, due to the relative smallness of the permeability κ, an order of magnitude less than that of the overpressure itself.

7. Conclusion

Identifying a quasi-steady burning regime applicable to the deflagration of confined porous energetic materials, it was demonstrated that the existence of an overpressure in the burned gas

region has a significant effect on the burned temperature, gas-velocity profile, and the burning rate of the material. In particular, it was shown, by an analysis of an appropriate model incorporating the primary aspects of two-phase flow in a porous material, that the burned temperature increases linearly, and hence the burning rate initially increases exponentially, with increases in the overpressure, followed by a more modest algebraic pressure dependence suggestive of Ap^n - type laws. This rapid increase in the burning rate, an explicit formula for which was derived, is in qualitative agreement with most experimental results on confined materials, which tend to show a sudden and rapid increase in the deflagration speed that is generally associated with the onset of convective burning. The present results lend further support to the concept that this transition is accompanied by gas permeation into the unburned material, the depth of which is generally less in magnitude than that of the overpressure itself. Thus, in contrast to the case of an unconfined deflagration, for which the gas flow relative to the condensed material is always in the downstream direction, the flow of gas in the unburned solid is, except in the limit of small overpressures, always directed in the upstream direction, providing an important mechanism for preheating the unburned material that results in an exponential increase in the burning rate.

Acknowledgement

This work was supported by the U. S. Department of Energy under Contract DE-AC04-94AL85000 and by a Memorandum of Understanding between the Office of Munitions (Department of Defense) and the Department of Energy.

References

1. Asay, B. W., Son, S. F., and Bdzil, J. B., The Role of Gas Permeation in Convective Burning, *Int. J. Multiphase Flow* 22:923–952 (1996).
2. Baer, M. R., and Shepherd, J. E., "A Thin Flame Model for Reactive Flow in Porous Materials," Sandia National Laboratories Report No. SAND83–2576, 1984.
3. Margolis, S. B., and Williams, F. A., Effects of Two-Phase Flow on the Deflagration of Porous Energetic Materials, *J. Propulsion Power* 11:759–768 (1995).
4. Baer, M. R., and Nunziato, J. W., A Two-Phase Mixture Theory for the Deflagration-to-Detonation Transition (DDT) in Reactive Granular Materials, *Int. J. Multiphase Flow*, 12:861–889 (1986).
5. Margolis, S. B., Williams, F. A., and Armstrong, R. C., Influences of Two-Phase Flow in the Deflagration of Homogeneous Solids, *Combust. Flame*, 67:249–258 (1987).
6. Taylor, J. W., The Burning of Secondary Explosive Powders by a Convective Mechanism, *Trans. Faraday Soc.* 58:561 (1962).
7. Probstein, R. F., *Physicochemical Hydrodynamics*, Butterworths, Boston, 1989, pp. 98–100.

Figure Captions

Fig. 1. Schematic illustration of deflagration in porous energetic material with two-phase flow in both the solid/gas and liquid/gas regions, with combustion occurring in the latter. An overpressure between the upstream (burned) and downstream (unburned) values of the gas pressure drives a permeation of the burned gases into the pores of the unburned solid.

Fig. 2. Final burned temperature T_b as a function of the overpressure $p_g^b - 1$. As the overpressure increases past a critical value, T_b changes from a decreasing to an increasing function of the porosity α_s.

Fig. 3. Burned gas velocity u_g^b as a function of the overpressure $p_g^b - 1$. Also shown is gas velocity $u_g(0)$ at the solid/liquid interface. Negative values indicate gas flow in the upstream direction, toward the unburned solid.

Fig. 4. Normalized burning-rate coefficient U_n as a function of the overpressure $p_g^b - 1$.

Fig. 5. Pressure profile $p(\xi)$ in the gas-permeation region for O(1) overpressures. Also shown is the velocity profile $u_g(\xi)$.

Fig. 6. Scaled pressure profile $P(\xi)$ in the gas-permeation region for large overpressures.

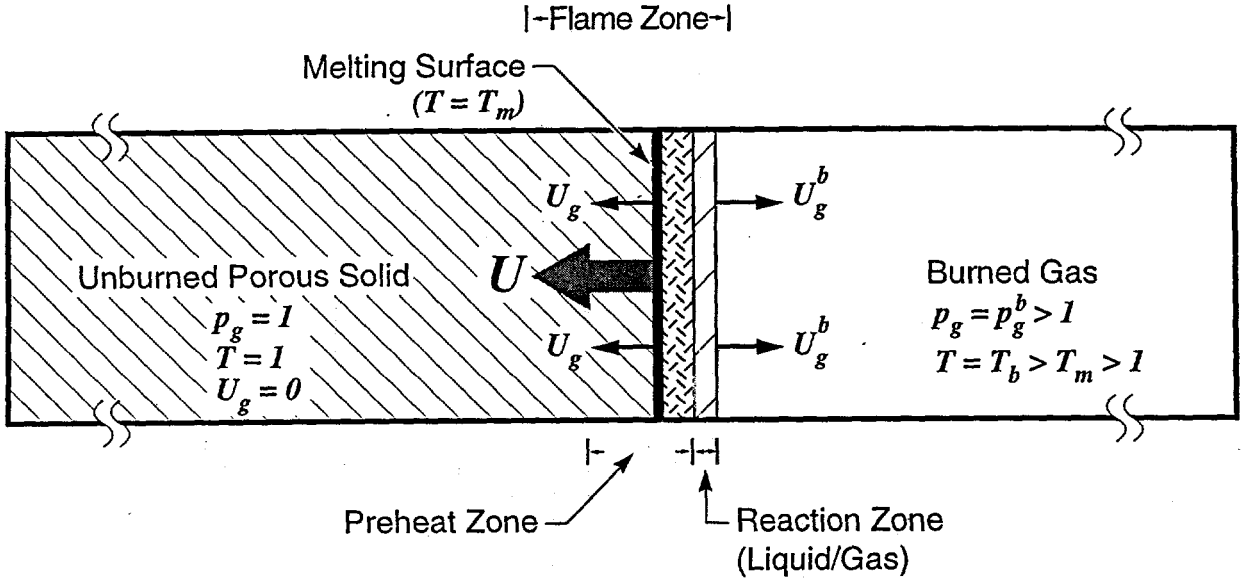
|-Flame Zone-|
Melting Surface
$(T = T_m)$
U_g
U_g^b
Unburned Porous Solid
$p_g = 1$
$T = 1$
$U_g = 0$
U
U_g
U_g^b
Burned Gas
$p_g = p_g^b > 1$
$T = T_b > T_m > 1$
Preheat Zone
Reaction Zone
(Liquid/Gas)

Figure 1

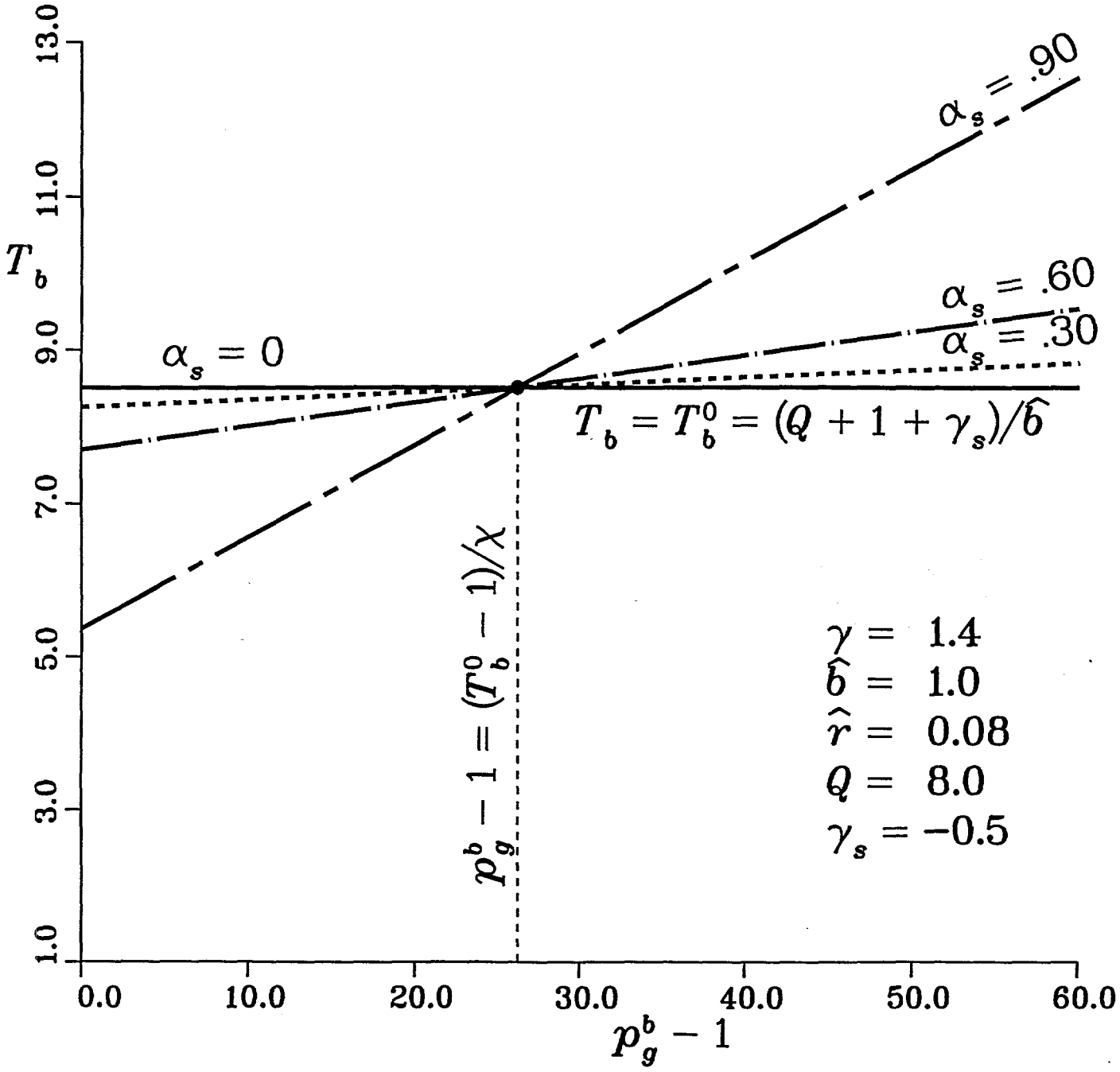
13.0
11.0
9.0
7.0
5.0
3.0
1.0
T_b
$\alpha_s = .90$
$\alpha_s = .60$
$\alpha_s = .30$
$\alpha_s = 0$
$T_b = T_b^0 = (Q + 1 + \gamma_s)/\hat{b}$
$p_g^b - 1 \equiv (T_b^0 - 1)/\chi$
$\gamma = 1.4$
$\hat{b} = 1.0$
$\hat{r} = 0.08$
$Q = 8.0$
$\gamma_s = -0.5$
0.0
10.0
20.0
30.0
40.0
50.0
60.0
$p_g^b - 1$

Figure 2

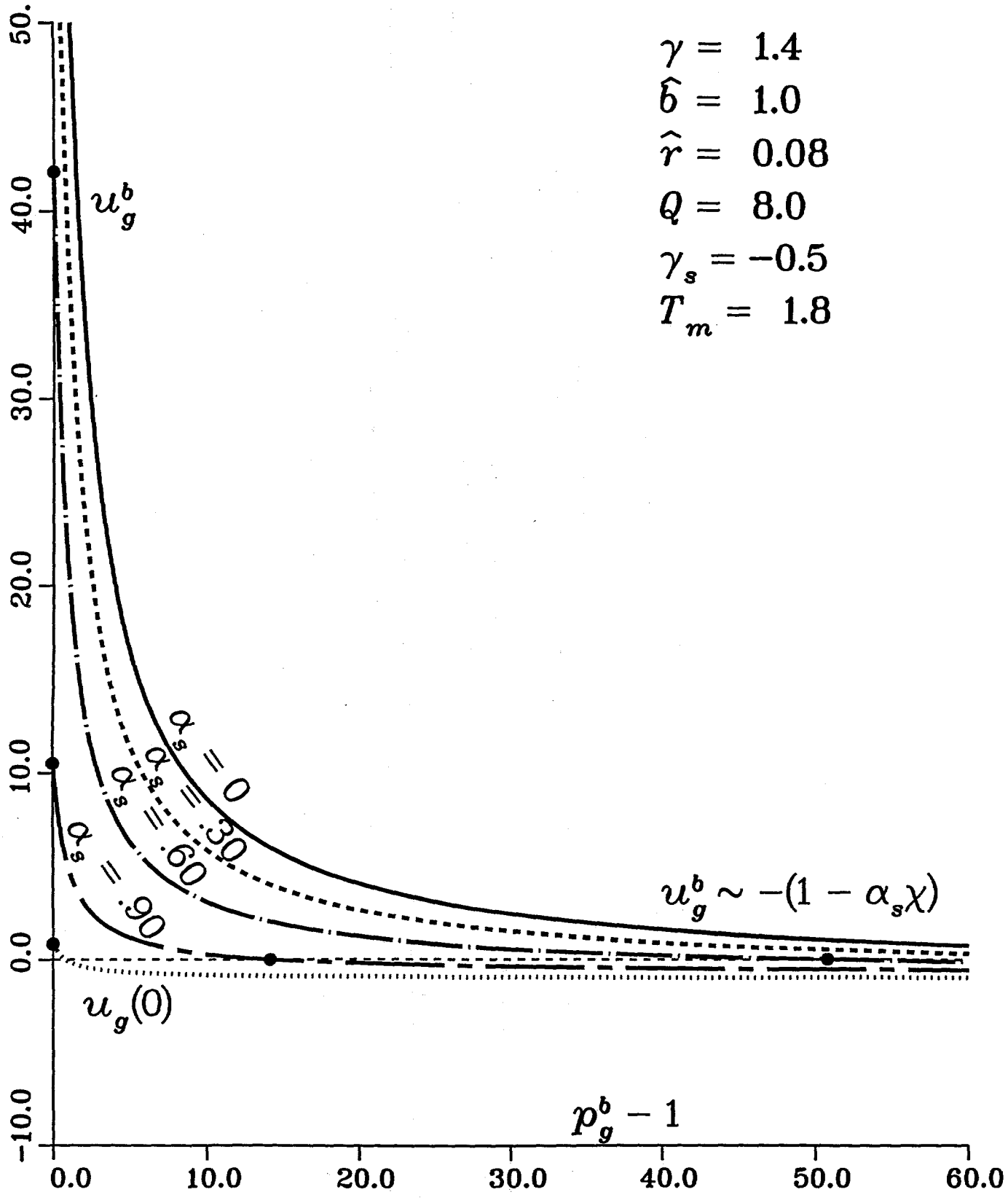
$\gamma = 1.4$
$\hat{b} = 1.0$
$\hat{r} = 0.08$
$Q = 8.0$
$\gamma_s = -0.5$
$T_m = 1.8$
u_g^b
$\alpha_s = 0$
$\alpha_s = .30$
$\alpha_s = .60$
$\alpha_s = .90$
$u_g^b \sim -(1 - \alpha_s \chi)$
$u_g(0)$
$p_g^b - 1$
50.
40.0
30.0
20.0
10.0
0.0
-10.0
0.0
10.0
20.0
30.0
40.0
50.0
60.0

Figure 3

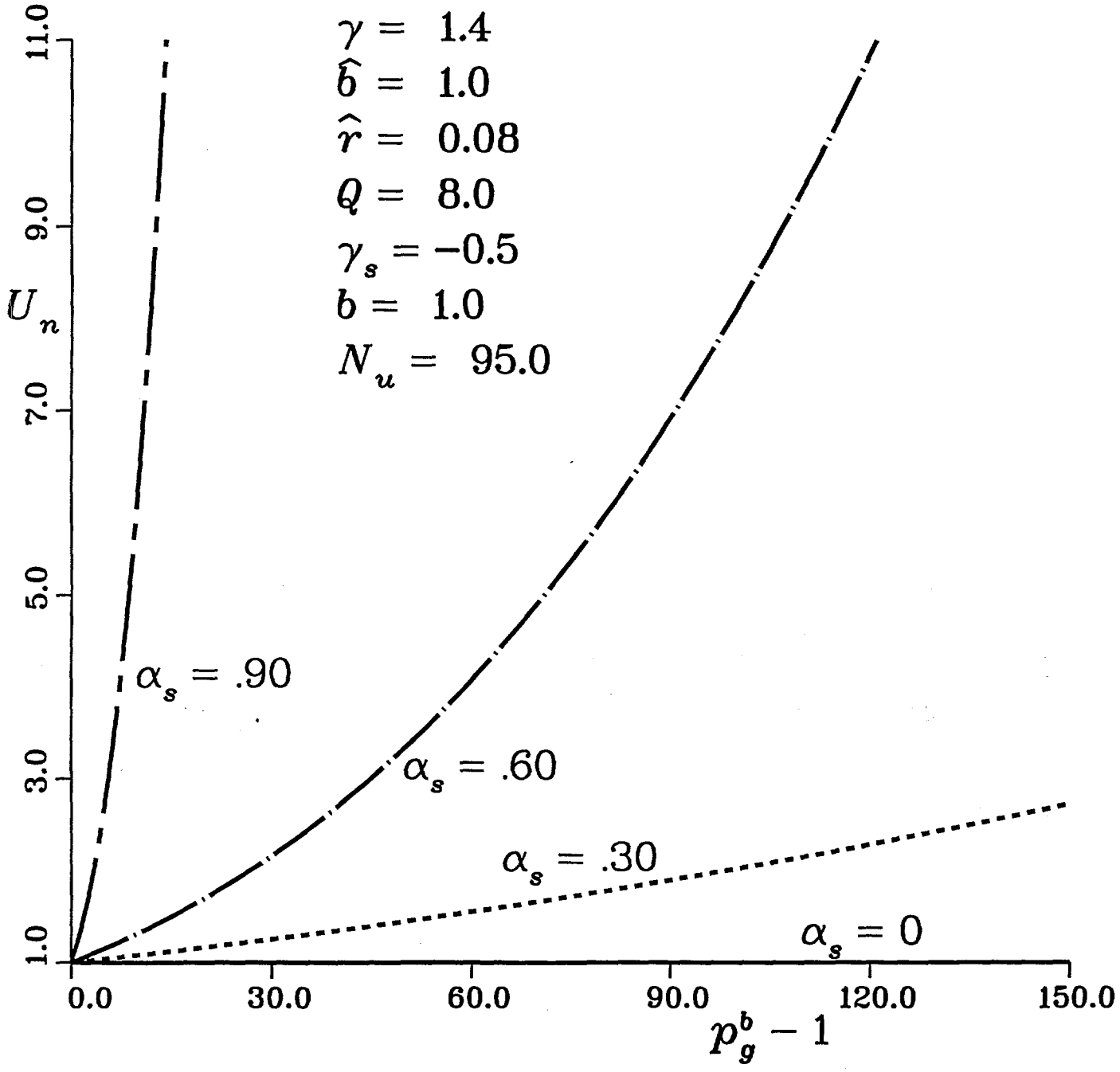
$\gamma = 1.4$
$\hat{b} = 1.0$
$\hat{r} = 0.08$
$Q = 8.0$
$\gamma_s = -0.5$
$b = 1.0$
$N_u = 95.0$
U_n
11.0
9.0
7.0
5.0
3.0
1.0
$\alpha_s = .90$
$\alpha_s = .60$
$\alpha_s = .30$
$\alpha_s = 0$
0.0
30.0
60.0
90.0
120.0
150.0
$p_g^b - 1$

Figure 4

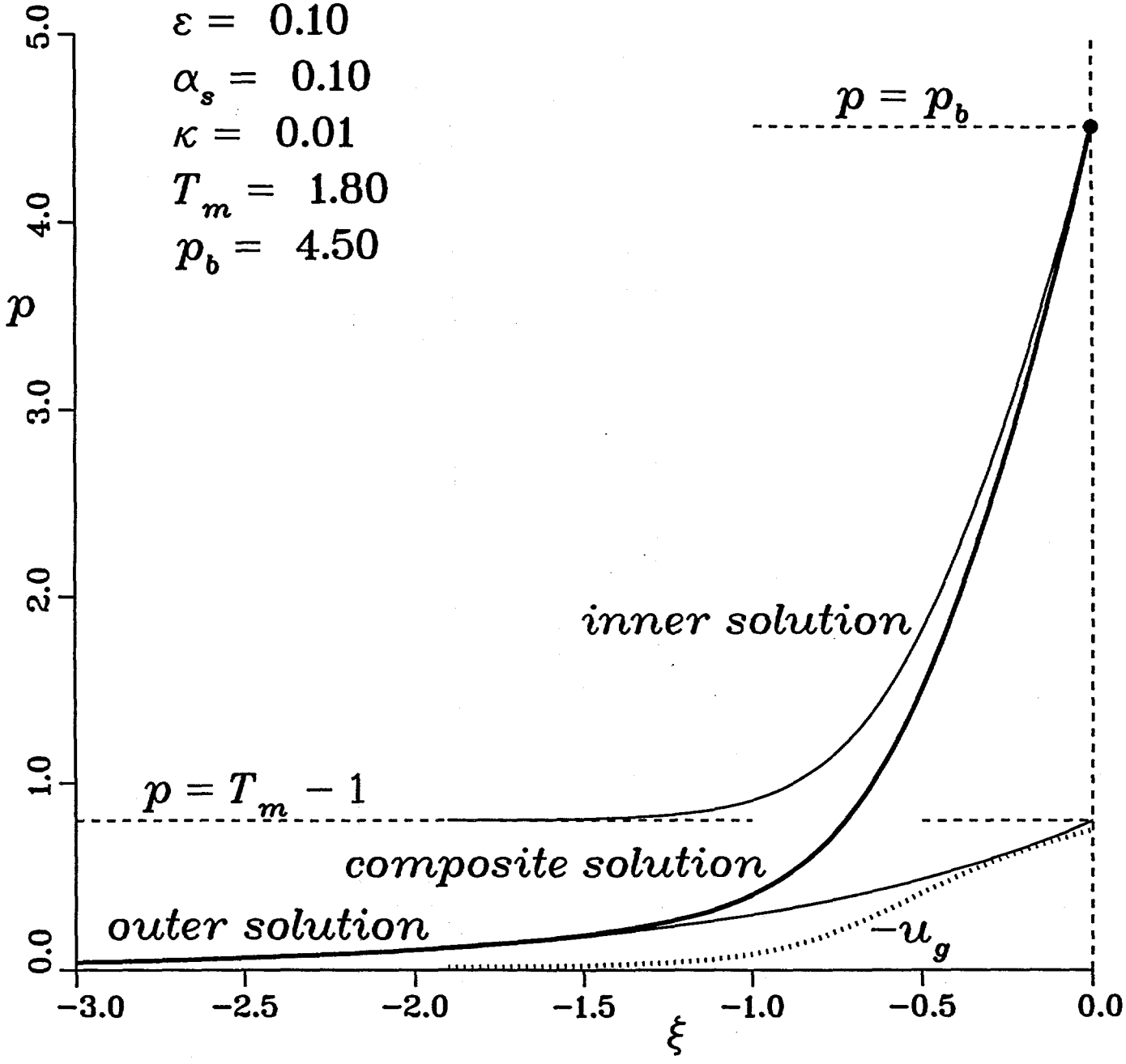
$\varepsilon = 0.10$
$\alpha_s = 0.10$
$\kappa = 0.01$
$T_m = 1.80$
$p_b = 4.50$
$p = p_b$
$p = T_m - 1$
inner solution
composite solution
outer solution
$-u_g$
p
ξ
5.0
4.0
3.0
2.0
1.0
0.0
−3.0
−2.5
−2.0
−1.5
−1.0
−0.5
0.0

Figure 5

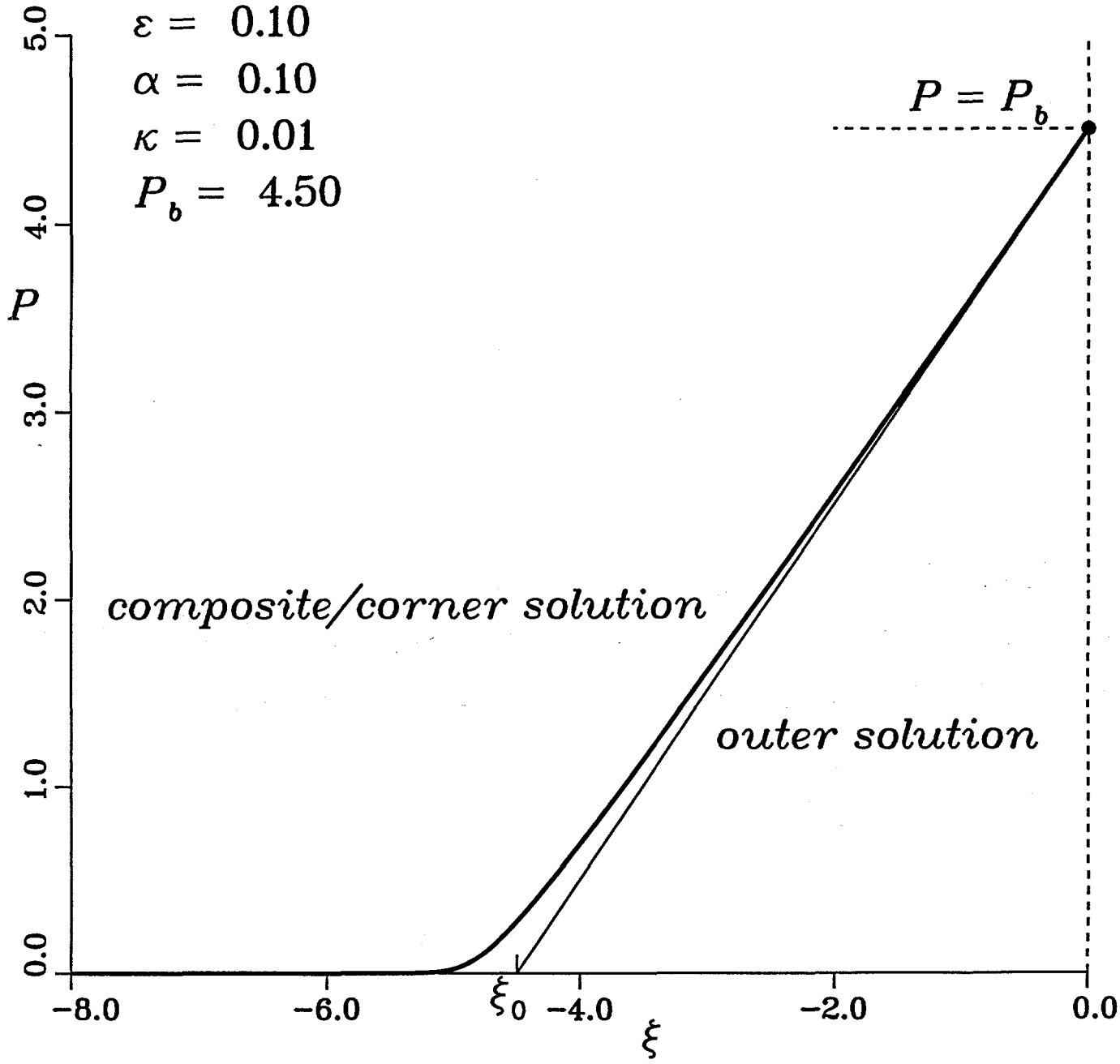
ε = 0.10
α = 0.10
κ = 0.01
P_b = 4.50
P = P_b
composite/corner solution
outer solution
P
ξ
ξ0
5.0
4.0
3.0
2.0
1.0
0.0
−8.0
−6.0
−4.0
−2.0
0.0

Figure 6

UNLIMITED RELEASE

INITIAL DISTRIBUTION

Dr. John K. Bechtold
Department of Mathematics
New Jersey Institute of Technology
Newark, NJ 07102-1982

Dr. Mitat A. Birkan
Program Manager
Directorate of Aerospace and Engineering Sciences
Department of the Air Force
Bolling Air Force Base, DC 20332-6448

Prof. Michael Booty
Department of Mathematics
New Jersey Institute of Technology
Newark, NJ 07102-1982

Prof. John D. Buckmaster
Department of Aeronautical and Astronautical Engineering
University of Illinois
Urbana, IL 61801

Prof. Sebastien Candel
Ecole Central des Arts et Manufactures
Grande Voie de Vignes
92290 Chatenay-Malabry
FRANCE

Dr. John Card
Department of Mechanical Engineering
Yale University
New Haven, CT 06520

Prof. J. F. Clarke
College of Aeronautics
Cranfield Institute of Technology
Cranfield-Bedford MK43 OAL
ENGLAND

Prof. Paul Clavin
Laboratoire Dynamique et Thermophysique des Fluides
Universite de Provence
Centre Saint Jerome
13397 Marseille Cedex 4
FRANCE

Prof. F. E. C. Culick
Jet Propulsion Center
California Institute of Technology
Pasadena, CA 91125

Prof. Martin Golubitsky
Department of Mathematics
University of Houston
University Park
Houston, TX 77004

Prof. Michael Gorman
Department of Physics
University of Houston
Houston, TX 77004

Dr. Daryl D. Holm
CNLS, MS 457
Los Alamos National Laboratory
Los Alamos, NM 87545

Prof. G. M. Homsy
Department of Chemical Engineering
Stanford University
Stanford, CA 94305

Dr. G. Joulin
Laboratoirie D'Energetique et de Detonique
Universite de Poitiers
Rue Guillaume VII
86034 Poitiers
FRANCE

Dr. Hans Kaper
Applied Mathematics Division
Argonne National Laboratory
9700 S. Cass Ave.
Argonne, IL 60439

Prof. A. K. Kapila
Department of Mathematical Sciences
Rensselaer Polytechnic Institute
Troy, NY 12128

Prof. D. R. Kassoy
Department of Mechanical Engineering
University of Colorado
Boulder, CO 80309

Prof. Joseph B. Keller
Department of Mathematics
Stanford University
Stanford, CA 94305

Prof. Barbara Keyfitz
Department of Mathematics
University of Houston
University Park
Houston, TX 77004

Prof. C. K. Law
Department of Mechanical and Aerospace Engineering
Engineering Quadrangle
Princeton University
Princeton, NJ 08544

Dr. Gary Leaf
Applied Mathematics Division
Argonne National Laboratory
9700 S. Cass Avenue
Argonne, IL 60439

Prof. Amable Liñán
Universidad Politecnica de Madrid
Escuela Tecnica Superior de Ingenieros Aeronauticos
Plaza del Cardenal Cisneros, 3
Madrid - 3
SPAIN

Prof. J. T. C. Liu
Division of Engineering, Box D
Brown University
Providence, RI 02912

Prof. Moshe Matalon
Department of Engineering Sciences and Applied Mathematics
Northwestern University
Evanston, IL 60208

Prof. Bernard J. Matkowsky
Department of Engineering Sciences and Applied Mathematics
Northwestern University
Evanston, IL 60208

Prof. A. C. McIntosh
Department of Fuel and Energy
University of Leeds
Leeds LS2 9JT
United Kingdom

Prof. D. O. Olagunju
Department of Mathematical Sciences
University of Delaware
Newark, DE 19716

Prof. R. E. O'Malley
Department of Applied Mathematics
University of Washington Seattle, WA 98195

Prof. Norbert Peters
Institute fur Allgemeine Mechanik
Technische Hochschule Aachen
Aachen
GERMANY

Prof. John Ross
Department of Chemistry
Stanford University
Stanford, CA 94305

Prof. Victor Roytburd
Department of Mathematical Sciences
Rensselaer Polytechnic Institute
Troy, NY 12128

Prof. W. A. Sirignano
Office of the Dean
School of Engineering
University of California, Irvine
Irvine, CA 92717

Prof. L. Sirovich
Division of Applied Mathematics, Box F
Brown University
Providence, RI 02912

Prof. G. I. Sivashinsky
Department of Mathematics
Tel-Aviv University
Ramat-Aviv, Tel-Aviv 69978
ISRAEL

Prof. Mitchell D. Smooke
Department of Mechanical Engineering
Yale University
New Haven, CT 06520

Prof. D. Scott Stewart
Department of Theoretical and Applied Mechanics
University of Illinois
Urbana, IL 61801

Prof. C. H. Su
Division of Applied Mathematics, Box F
Brown University
Providence, RI 02912

Prof. Cesar Treviño
Departmento de Termica y Fluidos
Universidad Nacional Autonoma de Mexico
Facultad de Ingenieria
Patios No. 12, Jardines del Sur
MEXICO 23, D.F.

Prof. Vladimir Volpert
Department of Engineering Sciences and Applied Mathematics
Northwestern University
Evanston, IL 60208

Dr. David Weaver
Air Force Rocket Propulsion Laboratory
DYP/Stop 24
Edwards Air Force Base, CA 93523

Prof. Forman A. Williams
Department of Applied Mechanics and Engineering Sciences
University of California, San Diego
La Jolla, CA 92093

Prof. Vigor Yang
Department of Mechanical Engineering
Pennsylvania State University
University Park, PA 16802

Prof. Benn Zinn
Department of Aerospace Engineering
Georgia Institute of Technology
225 North Avenue, NW
Atlanta, GA 30332

C. K. Westbrook, LLNL, L-321

MS 1110 R. C. Allen, 1422
MS 0834 A. C. Ratzel, 9112
MS 0834 M. R. Baer, 9112
MS 0834 M. L. Hobbs, 9112
MS 0834 R. J. Gross, 9112

MS 9001 T. O. Hunter, 8000
MS 9405 R. E. Stoltz, 8008
MS 9004 M. E. John, 8100
MS 9213 S. C. Johnston, 8103
MS 9054 W. J. McLean, 8300
MS 9163 W. Bauer, 8302
MS 9042. C. M. Hartwig, 8345
MS 9056 L. A. Rahn, 8351
MS 9051 W. T. Ashurst, 8351
MS 9051 A. R. Kerstein, 8351
MS 9052 D. R. Hardesty, 8361
MS 9055 R. Behrens, 8361
MS 9052 S. B. Margolis, 8361 (30)
MS 9053 R. W. Carling, 8362
MS 9021 Technical Communications Department, 8815, for OSTI (10)
MS 9021 Technical Communications Department, 8815/Technical Library, MS 0899, 4414
MS 0899 Technical Library, 4414 (4)
MS 9018 Central Technical Files, 8950-2 (3)